Desalination and Water Treatment
www.deswater.com

doi:10.5004/dwt.2019.23476

141 (2019) 23–35
February

Simulation and optimization study of the humidification–dehumidification desalination process

Faissal Abdel-Hady[a,*], Mohammed Alghamdi[a], A.K. Mazher[b], Abdulrahim Alzahrani[a]

[a]*Chemical and Materials Engineering Department, King Abdul-Aziz University, Jeddah, Saudi Arabia, email: faissalhady@gmail.com (F. Abdel-Hady), MOHAMMED_MOGHRAM@hotmail.com (M. Alghamdi), aaoz77839@gmail.com (A. Alzahrani)*
[b]*Nuclear Engineering Department, King Abdul-Aziz University, Jeddah, Saudi Arabia, email. ben.muzhar@gmail.com (A.K. Mazher)*

Received 19 February 2018; Accepted 17 November 2018

ABSTRACT

The humidification–dehumidification method (HDH) is a thermal desalination process. The process is viewed as a promising technique for small-capacity production plants. The process has many features, which include operation at low temperatures and the ability to combine with a sustainable solar-energy source. This paper demonstrates the design, modeling, simulation, economy, and optimization of an HDH desalination unit simulated within one hour of operation. The designed unit has continued water circulation across the humidifier (HD), a cross-flow oil heater, and closed air circulation. The effects and economic impact of a circulating air-mass flow rate and HD-inlet water temperature on unit productivity are studied. Other parameters, such as energy consumption, heat-to-mass transfer ratio, humidifier enthalpy difference, humidifier thermal efficiency, gained-output ratio (GOR), and annual production costs, are evaluated. Experimentally obtained mass-transfer coefficients in the humidifier were used to simulate the desalination unit. The study reveals that increasing air-mass flow rate has a significant effect on improving unit productivity. Moreover, highest productivity was obtained at the maximum simulated humidifier-inlet water temperatures. Packing with a higher mass-transfer coefficient gives higher unit productivity. The unit was optimized to achieve the best operating conditions, with higher productivity, at lower operating costs, maintaining best energy use at the highest attainable GOR. The optimal operating air-mass flow rate for all conditions ranged between 0.131 and 0.1998 kg/s for both the experimental and the simulated conditions. The lowest production cost obtained was at the HD-inlet water temperature of 50°C. The best experimental production costs were US$/0.07/L compared to US$0.066/L for the simulation. Finally, the simulation process showed good agreement with the experimental results, which can be a useful tool to further evaluate the unit when coupled with a renewable-energy source.

Keywords: Desalination; Humidification; Dehumidification; Design; Simulation

1. Introduction

With the increase in population, the need for freshwater has become a crucial issue that has to be resolved. Most global fresh water is purified and treated to make it suitable for human use. Natural sources of available fresh water are not enough, especially in the Middle East; hence, looking for desalination processes is very important to provide drinkable water to match the development of areas and meet population demands. Several desalination processes have already been implemented in the Middle East, which have proven their capabilities in commercial production and the quality of distilled water. These methods are thermal, either using dual-purpose thermal plants or the membrane desalination technique. Multistage-flash-desalination (MSF), multi-effect-desalination (MED), vapor-compression (VC), and reverse-osmosis (RO) plants are the most common desalination techniques in the region. Fifty percent of the world's desalinated water comes from the membrane desalination process, and the rest is generated thermally.

*Corresponding author.

MSF plants represent 85% of the thermal units' output, and RO plants have 90% capacity for the membrane process [1]. Such processes are used commercially to serve populations living in residential areas and modern developed cities. In arid regions, large-scale desalination cannot be used due to economic ineffectiveness; hence, smaller-scale effective methods are used. The humidification–dehumidification desalination process (HDH) can be the most suitable process for arid regions due to its simplicity. It uses low amounts of power, low temperature, and low-pressure water flow for the production of fresh water. The constructional design of the HDH process is a significant research domain for desalination-technology development. There are many publications that focus on the design of the HDH process to improve its effectiveness [2,3]. Such a method could be more cost-effective when solar energy is coupled with the HDH process, and in other hybrid-system desalination processes [4,5]. However, it is necessary to study the full range of constructional arrangement of the HDH process to evaluate its capacity to meet the essential purpose of high productivity and applicability for people in decentralized areas. Modeling and simulation can provide the required data for HDH desalination, which can be used for economic evaluation and process optimization. The simulation and experimental studies provided results in terms of the maximum attainable productivity at the lowest possible production cost.

The HDH desalination system can be integrated with other desalination systems or renewable-energy sources. González et al. [6] implemented a multi objective optimization formulation for designing an integrated desalination system. Optimization provides the best configuration and reveals the benefits of integrating a thermal desalination process, such as MSF/MED, in the thermal membrane-distillation process. Performance improvement is successfully attained using the waste-heat recovery system, which can be implemented during the HDH process. With different components and operation modes, the HDH process can be optimized to the best arrangement and operating conditions. The HDH process can integrate with other desalination technologies used in Gulf Cooperation Council (GCC) countries where fresh water is extremely limited. The water network in such countries can be optimized using the approach of an integrated design and an operation macroscopic water network [7]. Water uses, storage, and transportation costs are operationally and economically optimized. Further economic improvement is expected when the system integrated with the HDH process is coupled with a renewable-energy source from recycled wastewater streams.

Fig. 1 shows the system designed with both air and water circulation. Air circulates in a closed system, and water circulation across the humidifier needs makeup water for compensation. Closed air circulation is established to avoid the continued loss of thermal energy; similarly, losses on the water side are reduced by providing only makeup water less proportionally to the rate of circulation. One of the motivations for studying such a system is the need for a simple desalination technique serving arid areas with an energy supply with the fewest possible process complications using locally available materials, such as synthetic motor oil, instead of using expensive thermal fluids. The study provides the baseline for system analysis of air and water routes with electrical power as their energy source. However, this could be improved by replacing the electrical energy source with a low-grade waste-heat source or renewable-energy source.

2. Mathematical model

The following assumptions were employed to develop the mathematical model for the HDH desalination unit:

1. The system operates under steady-state conditions during each time step.
2. The system works under atmospheric pressure.

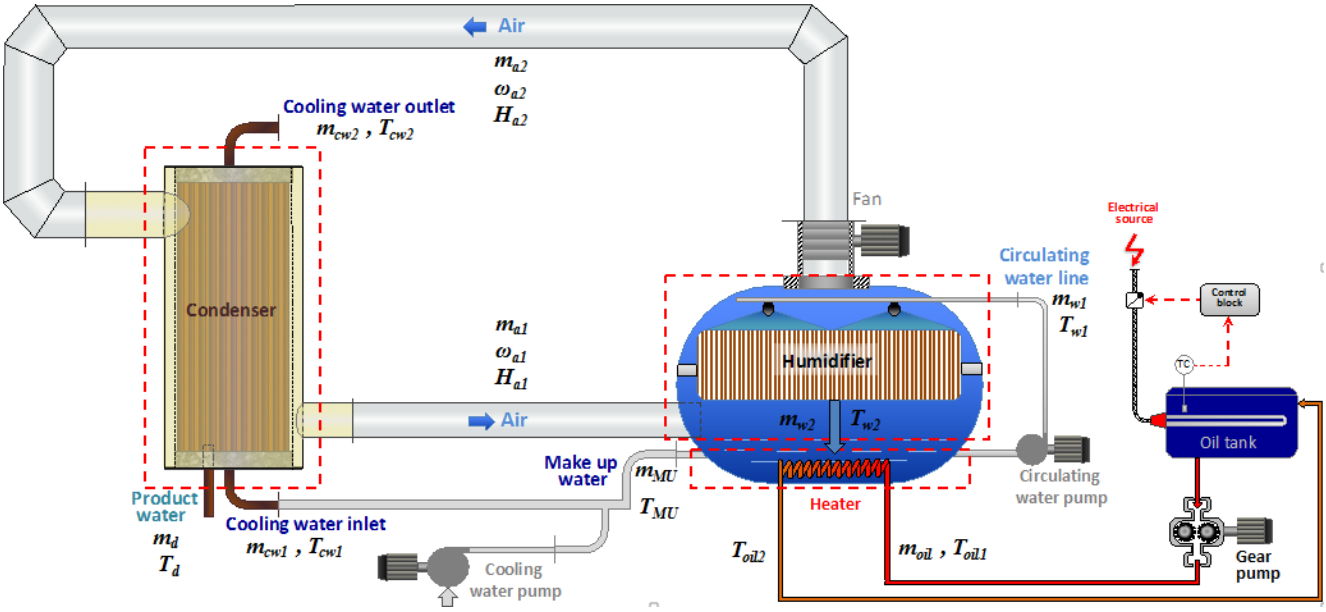

Fig. 1. Humidification–dehumidification desalination unit.

2.1. Humidifier

In the humidification process, hot water is brought into contact with flowing air using different packing types and arrangements to increase air humidity. The more sensible heat from water, the more absolute humidity is obtained at the air-side. In such a process, mass and heat transfer are toward the air-side. For the air–water system under normal conditions and entirely wet packing, the *Lewis* number is $le = \frac{a}{D_{AB}}$ equal to unity [8,9], and the Lew is analogy $\frac{ha}{K_y c_a} = le^{\frac{2}{3}}$ [10] is equal to one; this was also applied in other air–water-system analyses [11]. Then, the design equation for the humidifier is:

$$Z = \int_{H_{a1}}^{H_{a2}} \frac{m_a dH}{SK_y a\left(H_i - H\right)} \tag{1}$$

In order to solve the previous equations, it is required to stepwise the calculation from point to point throughout the humidifier, or it can be solved graphically using the Mickley method by the reversely stepwise construction of the equilibrium and operating curves.

For model simplicity, H. Jaber et al. [12] developed equations based on the effectiveness number of transfer units (ε-NTU) method. The solution obtained by ε-NTU successfully revealed less error when compared to the approach used by Chebyshev [13]. The application of the Chebyshev method to the Merkel equation gives the integrand sum at predetermined values within the integration interval by multiplying a constant by interval times, which provides the desired approximate integral.

It was also compared with the log mean enthalpy difference (LMED) method and obtained good agreement with no significant errors. The LMED method can be used where inlet conditions are known for the iterative model, as in the present work.

From design Eq. (1), the enthalpy integral can be changed to LMED, where correction factor *f* is applied to correct for the nonlinearity of saturated air enthalpy:

$$f = \frac{H_{as1} + H_{as2} - 2H_{avg}}{4} \tag{2}$$

Applying the correction factor to the system, LMED gives the following equation:

$$\Delta Hm = \frac{\left(H_{as2} - H_2\right) - \left(H_{as1} - H_1\right)}{\ln\left(\frac{\left(H_{as2} - H_2\right) - f}{\left(H_{as1} - H_1\right) - f}\right)} \tag{3}$$

The modified humidifier-design equation can be expressed as the following [14–17]:

$$m_a\left(H_2 - H_1\right) = K_y a V \Delta H_m \tag{4}$$

In this process, the enthalpy difference across the humidifier indicates the capability of the humidifier to transfer more vapor to the air towards the dehumidifier, which is the driving force for the humidification process and its capacity for higher distillate production.

2.2. Dehumidifier

Mizushina et al. [18] developed a method that can be used when water vapor is condensed. It is based on the simultaneous heat- and mass-transfer problem, which can be solved by the same procedure for direct-contact equipment. The required surface area for a given performance can be computed with the following relation [19]:

$$ADH = \frac{m_a}{K_M} \int_{H_{a1}}^{H_2} \frac{dH}{\left(H_i - H\right)} \tag{5}$$

Eq. (5) can be solved by stepwise point-to-point calculation and graphically presented similarly to the humidifier solving technique. An iterative form of this equation is plugging in the desalination-unit model and applying an LMED type of heat-exchanger analysis to the system, where K_M corresponds to U in the heat exchanger and the balance is taken to the water side, while considering U as an overall heat-transfer coefficient representing the total of all resistances.

Then, the mathematical model of the dehumidifier is given by:

$$m_{cw} C_{cw}\left(T_{cw2} - T_{cw}1\right) = UA_{DH}\Delta T_{lm} \tag{6}$$

where the logarithmic mean temperature difference is taken as follows [20]:

$$\Delta T_{lm} = \frac{\left(T_{a2} - T_{cw2}\right) - \left(T_{a1} - T_{cw1}\right)}{\ln\left(\frac{T_{a2} - T_{cw2}}{T_{a1} - T_{cw1}}\right)} \tag{7}$$

LMED use is valid for the present heat exchanger, with one shell pass and one tube pass, as well as in multiple numbers of shell and tube passes; flow through the heat exchanger is not fully concurrent or fully counter current.

3. Solution procedure

The model is solved in the steady-state condition of each run. Design equations, formulated in an Excel spreadsheet and a generalized reduced gradient (GRG) algorithm, used to optimize the objective of each constraint intersection [21], were implemented. The lower- and upper-bound constraints are specified in the solver to retrieve the objective solution. The GRG nonlinear solver reveals extensive sensitivity analysis that is better than linear programming [22]. This technique was previously used in the optimization of a complex plant [23] and, recently, in the optimization of industrial gas-supply networks [24]. In order to solve the model for the desalination unit, the main parameters were set to be within a small variation in airflow. The humidifier had a constant inlet circulating water flow rate. In the dehumidifier, the cooling water flow rate was constant. These parameters are shown in Table 1.

Based on the developed energy-balance equations and input-design parameters, Eqs. (4), (6), (33), and (34) were solved simultaneously by an iterative procedure for both humidifier and dehumidifier energy equations. Initial guesses were given for T_{a1}, T_{a2}, T_{w2}, and T_{cw2}. For each set of

Table 1
Basic design parameters

Parameter	Value	Unit
A_{DH}	5.817	m^2
m_{cw}	0.2831	Kg/s
m_w	0.571	Kg/s
c_w	4178	J/kg°C

airflow rate, several runs for different humidifier-inlet temperatures were implemented to calculate desalination-unit productivity. The produced water was obtained in kilograms per hour.

4. Results and discussion

The desalination unit was simulated at different humidifier-inlet water temperatures and airflow rates. The mass-flow-rate ratio was varied by changing the airflow rate and fixing the water flow rate at a maximum of 0.571 kg/s. Mass-flow-rate ratios ranged from 2.8 to 19.7. Moreover, the system was water-heated; hence, airflow variation enabled the study of the sensible-heat effect from the water to the flowing air, thereby optimizing the design. The control of the humidification process by variable airflow revealed the optimal sufficient contact time for air to become saturated [8]. An HDH design of an experimental (DOE) study conducted by Farsad et al. [25] showed the possibility of producing distillate at different condenser characteristics for a fixed air-mass flow rate. This was attributed to the contradictory effect of the inlet water flow rate. The design, operating data of the desalination unit, and simulated results for one hour of operation are discussed. The process was analyzed as a steady condition at fixed heating conditions unlike the dynamic behavior when the process is coupled with a solar-energy source [26].

4.1. Effect of airflow rate and humidifier-inlet water temperature

The objective was to study the productivity of the desalination unit by changing one operating parameter, either airflow rate or inlet water temperature, during each run. The effects of air- and water flow rate are complicated and depend on the design of the process where optimal values could be obtained; therefore, further simulation research was recommended by Kabeel et al. [27]. Fig. 2 illustrates the variation of unit productivity at different airflow rates; it also shows simulation results obtained at different humidifier-inlet water temperatures. The results allowed us to compare the simulation outputs with the experimental data of the same designed unit [28]. Airflow was simulated as low as 0.089 kg/s, and the maximum airflow rate was 0.1998 kg/s. At a constant inlet water flow rate and temperature to the humidifier, the amount of produced water increased with an increasing airflow rate. Fig. 2 shows the gradual increase of productivity during the simulation. The increase in system productivity was not sustained, depending on humidifier-inlet water temperature and airflow rate. The increase of airflow rate enhanced

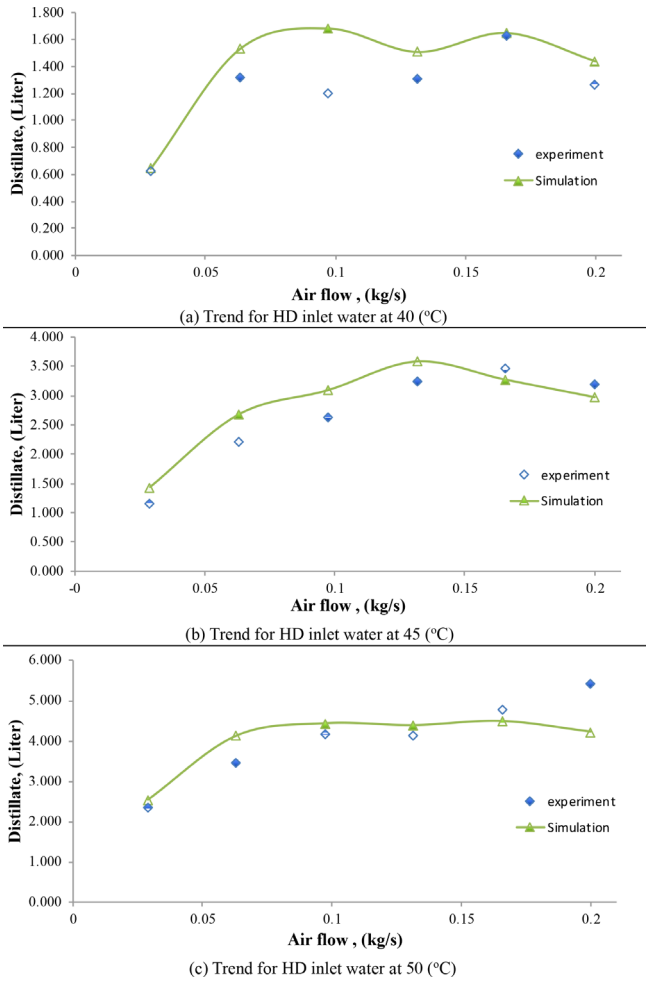

Fig. 2. Productivity at different airflow rates.

the cooling effect of the process; therefore, it required more heating to ensure higher productivity at a higher airflow rate. Moreover, residence time was reduced for the humidification to take place at a higher airflow rate and, eventually, both humidifier efficiency and enthalpy difference were decreased. The results of the simulation show a similar behavior with the experimental outputs. The maximum amount of produced water, when HD-inlet water temperature was 40°C and airflow rate was 0.166 kg/s, was 1.64 kg/h, while quantity increased severalfold, to 4.49 kg/h, for the same period and airflow rate at an HD-inlet water temperature of 50°C. When comparing the previous simulation output to the experimental yields for the same condition, the unit was capable of producing 1.62 kg/h when HD inlet water was 40°C, and 4.78 kg/h when HD inlet water was 50°C. The results show that, as humidifier-inlet water temperature increased, sensible heat from the water had good impact on the absolute humidity of the flowing air. The results also indicate that enthalpy difference increased as humidifier-inlet water temperature increased for both simulation and experimental outputs. The simulation output was in good agreement with the experimental output. The amount of produced water per hour indicates the improving capacity of unit production as more air is introduced to the system. This is attributed to the heating

and humidifying principle. Hence, more water vapor was entrained and diverted to the dehumidifier. This amount of produced water is promising when using renewable-energy sources, especially in arid areas.

4.2. Humidifier efficiency

The simulation curves shown in Fig. 3 are plotted and compared to the humidifier efficiency that was obtained experimentally. After the convergence of the model equations, Eq. (29) was used to calculate humidifier efficiency based on input and iterative results. Simulation results show that maximum humidifier efficiency was obtained at lower airflow rates regardless of inlet water temperature. Humidifier efficiency was calculated based on moist-air humidity at its inlet and outlet. The solution obtained results at lower airflow rates, where humidifier-outlet relative humidity (RH) is close to saturation conditions, $RH \approx 100\%$. This is due to longer air–water contact time at a low airflow rate. In the present design, water circulation was fixed at the maximum possible at 0.571 kg/s, and revealed a high water–airflow ratio of 19.7 at a low airflow rate, which enhanced the saturation condition. This result agrees with the experimental output, as the highest efficiency was obtained at a lower airflow rate and efficiency continued to decrease as airflow rate increased. Except for the low inlet water temperature of 40°C, experimental efficiency showed no significant change compared to the decreasing behavior of the simulated efficiency, which is attributed to the ideal conditions for the simulated data when compared to the experiment at a lower sensible-heat condition.

4.3. Humidifier thermal efficiency

Humidifier thermal efficiency was calculated by Eq. (31) for both the simulation and experimental analysis. This efficiency is usually used to measure the performance of various processes, such as heat engines, heat pumps, and refrigeration cycles. In the present work, humidifier thermal efficiency obeyed the second law of thermodynamics; hence, energy had a direction and degree of loss during the process. The humidifier operates between high-input heat-circulating water and low-temperature-circulating air. Fig. 4 illustrates humidifier thermal efficiency at different airflow rates. The results show the degree of conversion percentage of thermal input energy to the circulating air,

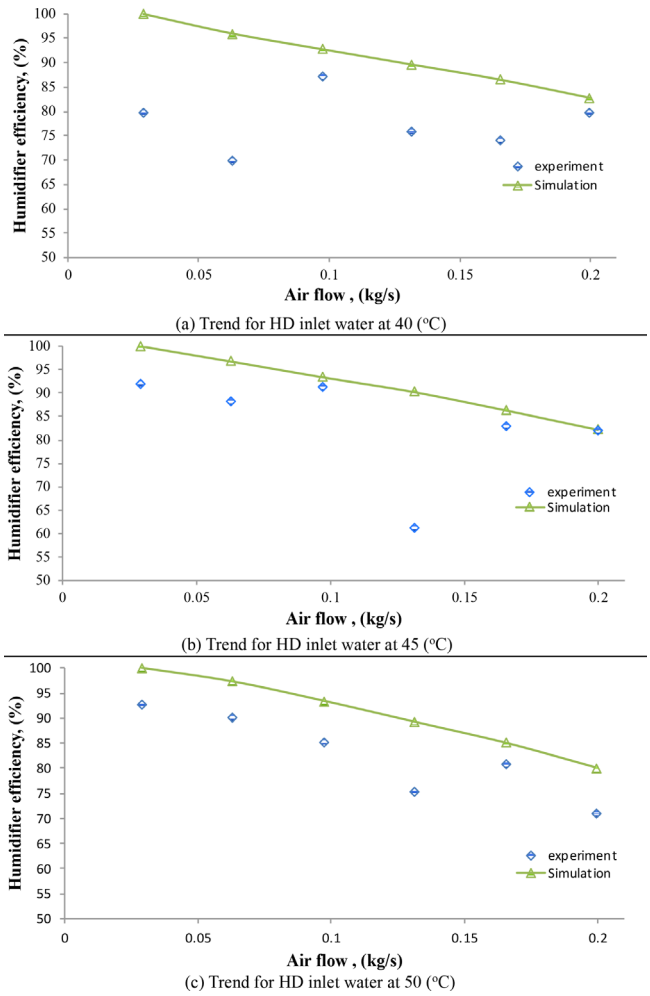

Fig. 3. Humidifier efficiency at different airflow rates.

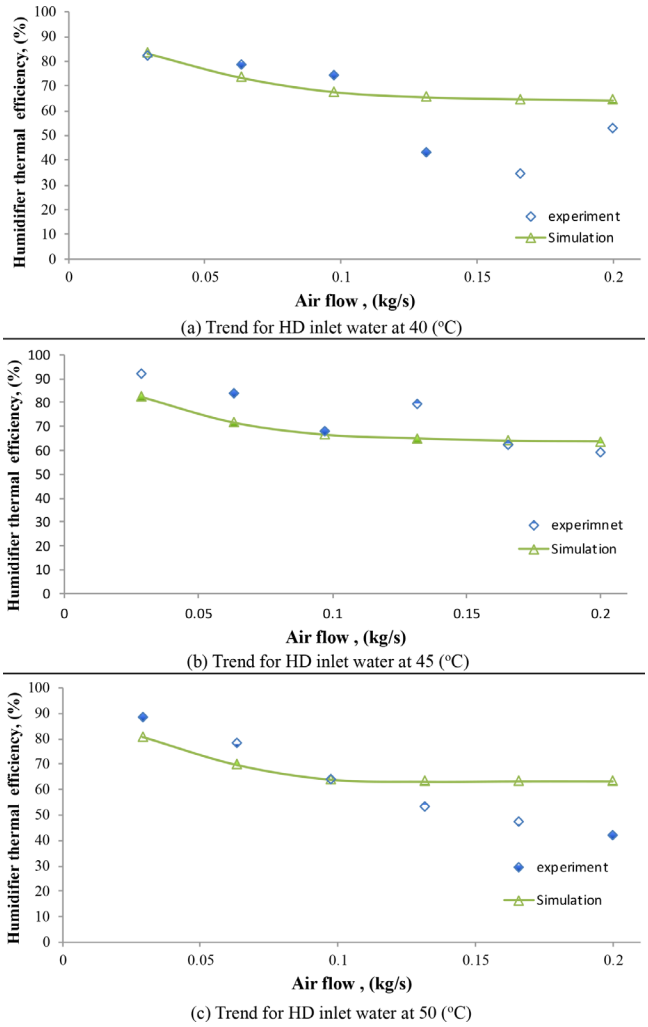

Fig. 4. Humidifier thermal efficiency at different airflow rates.

hence increasing humidification process capacity, which indicates the degree of "perfection" [29]. The energy-conversion percentage in the air side was shown to decrease as airflow rate increased in both the simulation and the experiment, which reveals lower thermal efficiency at higher airflow rates. Thermal efficiency became steadier, between 65% and 70%, in the simulation.

4.4. Gained output ratio (GOR)

The GOR indicates the thermal energy that the HDH desalination process consumes. The GOR value and process economics are usually considered during the design of the desalination units. A higher-GOR desalination system has higher capital costs and lower operating costs. The advantage of the present system, when coupled with solar energy, is that it makes the process economically feasible at lower GOR values. Fig. 5 illustrates GOR at different airflow rates simulated and compared with the experimental GOR values. In both experimental and simulation results, the GOR increased as airflow rate increased. The GOR increase was not continuously sustained as the airflow rate increased at the three HD-inlet water temperatures. The simulation outputs tended to have steady GOR behavior when the airflow rate reached 0.1 kg/s and higher. This behavior is attributed to the high-energy input in the simulation process and the slightly less energy required experimentally due to heating solar radiation on the humidifier body and ambient conditions. Moreover, sensible heat from the humidifier-inlet water temperature increased the system GOR.

4.5. System energy consumption

The energy input to the system was calculated and is illustrated in Fig. 6. The average energy input to the humidifier to maintain circulating water temperature at 40°C was 7.61 kWh in the experiment and 7.79 kWh in the simulation. The simulated energy consumption increased, on average, by 94.8% when the circulating water temperature increased from 40 to 45°C, compared to 116.7% obtained experimentally. This significant increase in energy consumption for humidifier circulating water, between 40 and 45°C, was reduced at higher circulating water temperatures. When the circulating water temperature increased from 45 to 50°C, it revealed 22.8% higher simulated energy consumption, and 12.3% obtained experimentally. This indicates a requirement

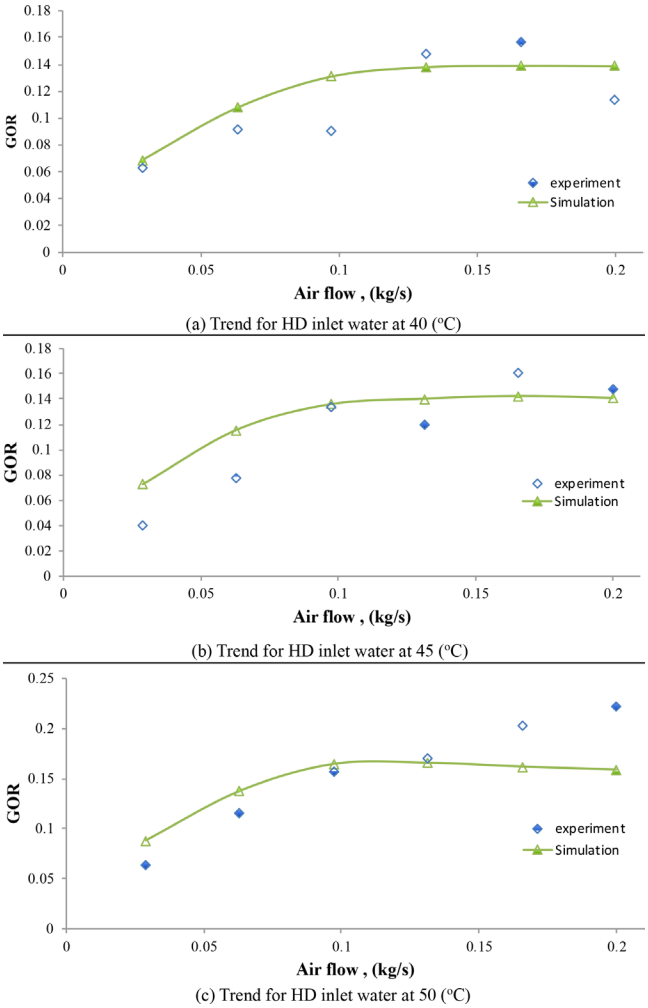

Fig. 5. GOR at different airflow rates.

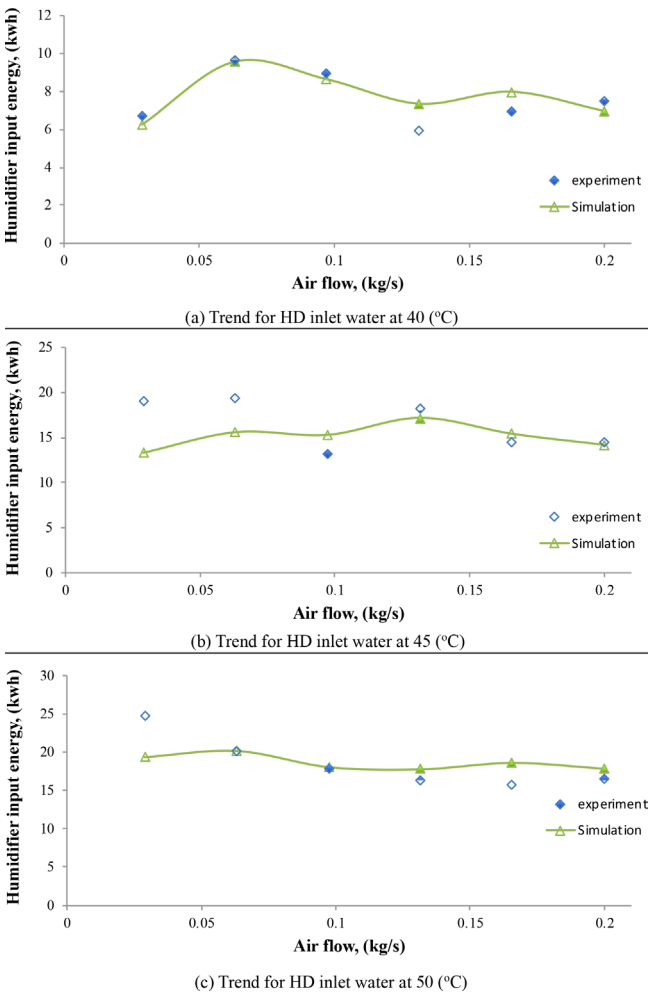

Fig. 6. Humidifier input energy at different airflow rates.

for less energy when a higher circulating water temperature is maintained with higher process productivity; hence, the process becomes more economically feasible. The average experimental input energy at 45°C circulating water temperature was 16.5 kWh, compared to 15.18 kWh obtained by simulation. Moreover, at 50°C circulating water temperature, average experimental energy consumption was 18.5 kWh, showing good agreement with the 18.64 kWh resulting from the unit simulation.

4.6. Annual production cost

Total operating cost is calculated based on the annual-cost method. The total operating cost of the system consists of the annual capital cost, annual maintenance cost, and annual operating cost. The annual capital cost was calculated for a 20-year investment and an interest rate of 5%. The capital cost of the system is US$4000. the maintenance cost was proposed as 3% of the annual capital charge [30], and the operating cost was obtained based on the variable operating cost. The variable operating cost is calculated based on the system energy-input price and the power consumed by drives and controls. The industrial-grade electrical-energy (kWh) cost in Saudi Arabia is about US$0.048 per kWh [31]. The designed unit was assumed to operate continuously throughout the year with 90% availability. The HDH process had less capital and operating costs when compared to high-temperature desalination systems with an accepted GOR for such a process. The total annual production costs for the simulated HDH process and the predicted one from the experiment runs are shown in Fig. 7. Both experimental and simulated conditions revealed a lower operating cost at higher airflow rates. Moreover, the operating cost was positively affected at a higher humidifier circulating water temperature. The average operating cost obtained experimentally was shown to be US$0.13/L at 40°C humidifier-inlet water temperature, and US$0.113/L for the simulated conditions. When the humidifier-inlet water temperature increased to 50°C, the operating cost was further reduced to US$0.07 and 0.066/L, on average, for the experimental and simulated conditions, respectively.

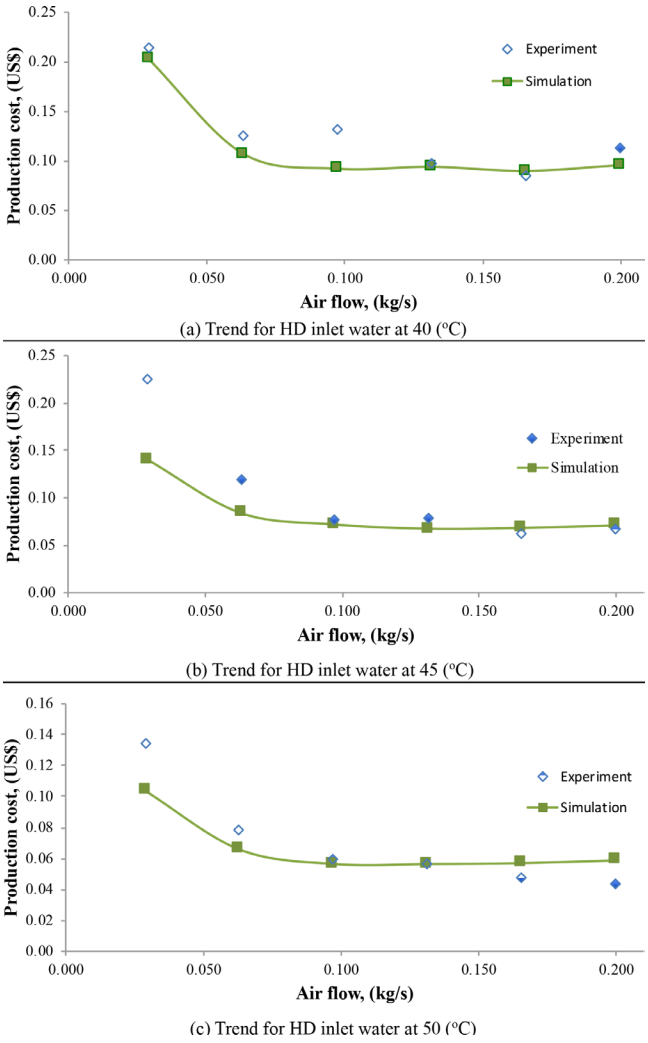

Fig. 7. Production cost at different airflow rates.

4.7. Optimization for operating cost, productivity, and GOR

Economic analysis of the process was used to optimize the design. Design optimization under the studied variations made for economic effectiveness under specific conditions [32]. Optimization could involve many objectives for energy requirements, cost reduction, or maximizing productivity [33]. Optimization is considered as a trade-off between different results to obtain optimal conditions for operating costs, system productivity, and the GOR. Percent-stacked bar graphs were constructed for each humidifier-inlet temperature at various airflow rates. The graphs shown in Fig. 8 represent the percentage amount of the operating cost, system productivity, and the GOR, which is a very useful tool to indicate the quantity percentage of each parameter in order to evaluate optimal conditions. The figure also shows experimental results, which were compared with the simulated conditions at each humidifier-inlet water temperature. In such a process, the trade-off between operating cost, system productivity, and the GOR is an important step to obtain the best conditions for highest productivity at lowest operating-cost conditions. The maximum attainable GOR is recommended to achieve the most economical energy consumption. When the humidifier-inlet water temperature was 40°C, optimal conditions were found to be an airflow rate of 0.166 kg/s for both experimental and simulated results. Unlike the previous condition, at a higher inlet water temperature of 45°C, optimal conditions were obtained at an airflow rate of 0.166 kg/s experimentally, and 0.131 kg/s for the simulated condition. Similarly, at 50°C, optimal operating conditions were obtained at 0.166 and 0.1998 kg/s for the experimental and simulated results, respectively. The results showed no significant difference between the simulated and the experimental results, which indicates a credible simulation process for predicting a process response at different conditions.

The current study is comparable with previous work in the field of HDH desalination. Table 2 shows the processes' power-supply type and the available data of the operated humidifier-inlet water temperature. Hourly system productivity and the results of the economic analysis are shown to evaluate the processes based on these factors. The present work shows a lower HD-inlet water temperature with

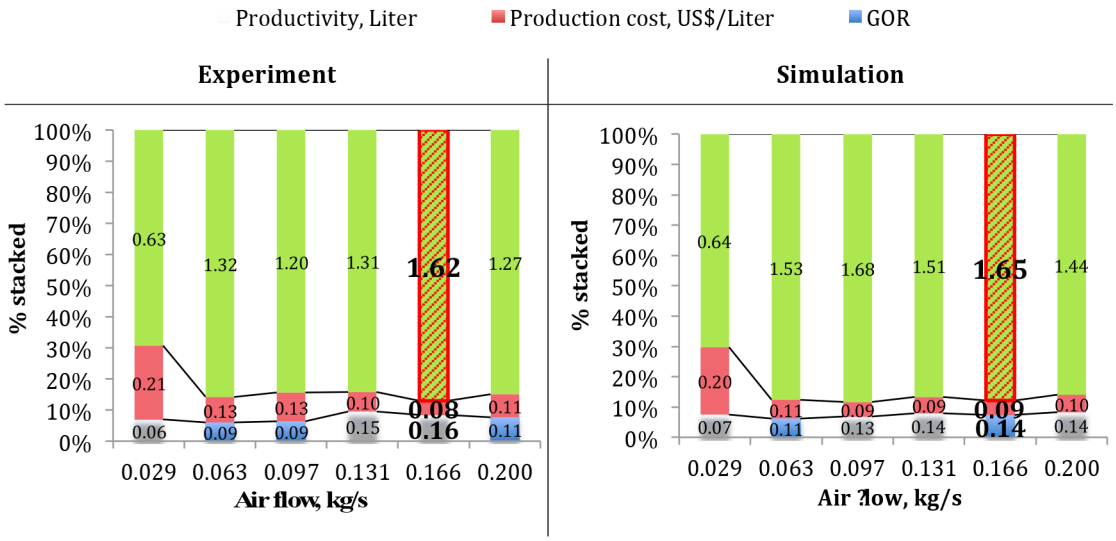

(a) Optimization at 40°C humidifier inlet water temperature.

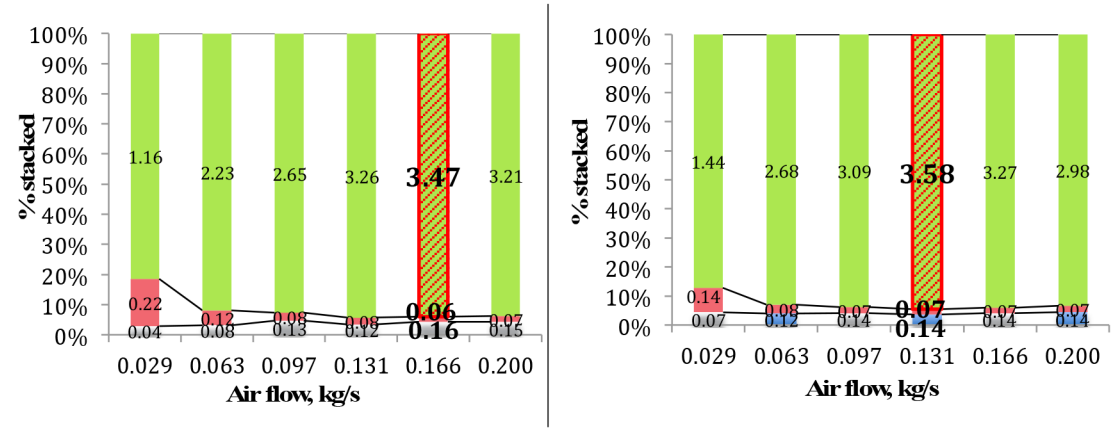

(b) Optimization at 45°C humidifier inlet water temperature.

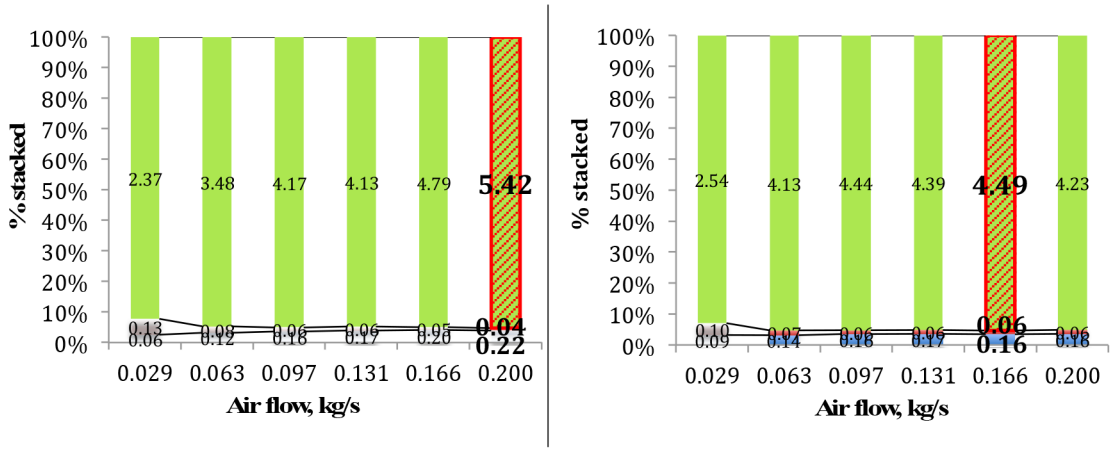

(b) Optimization at 50°C humidifier inlet water temperature.

Fig. 8. Optimization for the experimental and simulated conditions.

encouraging results regarding productivity and cost. Productivity of 4.49 kg/h is higher than most of the other work at 50°C HD-inlet water temperature. The capacity for production at a lower HD-inlet water temperature is attributed to closed air circulation and continuous HD water circulation, which reserves process heat. The incorporated HD bottom-oil-heated exchanger enhanced the speed-up heating rather than the separate storage-tank heaters. The stated system's ability is in favor of using the process when low-grade waste heat or solar energy is coupled with.

Table 2
Comparison of the present work with previous results

Reference	Description	Humidifier-inlet water temperature, °C	Productivity kg/h	Cost US$/L
Rajaseenivasan et al. [34]	A biomass-powered bubble column humidification–dehumidification desalination system. Saw-dust briquettes were used as biomass fuel.	60	6.1	0.0133
Deniz et al. [35]	Solar water and air heaters with photovoltaic panels for electrical energy.	58.5	0.87 mx	0.0981
Ahmed et al. [36]	Humidification–dehumidification desalination process (HDH) with new corrugated packing aluminum sheets in the humidifier. Water was heated in a storage tank by electrical power.	49	15	0.01
El-Agouz [37]	Compressed air passed through a seawater-bubble column heated by electrical power.	86	8.22	0.115
Rahimi-Ahar et al. [38]	Evacuated tube water solar collector; flat-plate air solar collector; humidification at subatmospheric pressure and dehumidification at atmospheric pressure.	77	2	0.04
Hamed et al. [39]	Solar humidification–dehumidification desalination unit by evacuated tube collectors.	87 max	2.75 per m^2	0.0578
Behnam et al. [40]	HDH solar desalination system equipped with a combination of a heat pipe, evacuated tube collector, and air-bubble column humidifier.	–	0.9	0.028
Shafii et al. [41]	Hybrid HDH desalination system integrated with a heat pump to raise the temperature of the air entering the humidifier.	–	2.79	0.0114
Current work	Closed air circulation, humidifier water circulation with makeup, and electrically heated oil as energy source.	50	4.49	0.066

5. Conclusion

A numerical simulation was performed for a humidification–dehumidification desalination unit. It aimed to investigate the effect of various parameters, such as humidifier circulating water, airflow rate, and humidifier characteristics, on the HDH desalination system. The process was simulated under the prescribed conditions similar to the experimental humidifier-inlet water and dehumidifier cooling water temperatures. The following conclusions were drawn based on this study:

- Both experimental results and simulation outputs revealed higher humidifier efficiency at lower air-mass flow rates, positively affected by higher HD-inlet water temperature. The reduction of efficiency at higher airflow rates was attributed to the decrease of humidifier enthalpy difference for both cases. Moreover, higher humidifier-inlet water temperature had a positive effect on the humidifier enthalpy difference.
- The simulation and the experimental outputs showed that a higher air-mass flow rate adversely affected humidifier thermal efficiency and its capacity to perfectly use input energy in the system. The amount of energy consumed at a higher HD-inlet water temperature makes the process more economically feasible in terms of higher productivity per kWh.
- The GOR and annual production cost are important factors in obtaining optimal operating conditions. The GOR, obtained experimentally and by simulation process, increased as air-mass flow rate increased. Simultaneously, the annual production cost decreased. Maximum productivity at the lowest production cost and highest GOR of the unit was optimized. The optimal operating air-mass flow rate for all conditions ranged between 0.131 and 0.1998 kg/s. The higher the HD-inlet water temperature was, the higher the optimal air-mass flow rate. The lowest production cost obtained experimentally was US$0.07/L, compared to US$0.066/L for the simulation outputs when HD inlet water temperature was 50°C.

Finally, HDH appears to be a promising desalination process, especially for arid areas. Hence, the process was simulated at conditions similar to the experiment in order to evaluate the key performance parameters of the HDH desalination process. The results show that possible

improvement could be expected when an HDH unit is powered by a renewable-energy source due to good productivity and economic outcomes at a low humidifier-inlet water temperature.

Acknowledgments

This project was funded by the National Plan for Science, Technology, and Innovation (MAARIFAH) of King Abdulaziz City for Science and Technology, Saudi Arabia (award number 11-ENE2004-03). The authors also acknowledge with thanks the Science and Technology Unit at King Abdulaziz University for their technical support. The authors acknowledge the great support of Dr. Abdulsalam Alghamdy, head of the King Salman Energy Chair in accommodating the project installation in their premises.

Symbols

A	—	Area m^2
C_A	—	Annual capital cost *US$*
C_M	—	Maintenance cost *US$*
C_{OP}	—	Operating cost *US$*
C_{TOP}	—	Total operating cost *US$*
D_{AB}	—	Mass-diffusion coefficient of air in water m^2/s
H	—	Enthalpy *kJ/kg*
K_M	—	Dehumidifier mass-transfer coefficient $Kg/m^2\ s$
K_y	—	Gas-phase mass-transfer coefficient of humidifier $Kg/m^2\ s$
M	—	Mass flow rate per unit length of perimeter *kg/m s*
N_t	—	Total number of tubes
P	—	Capital cost *US$*
Pr	—	Prandtl number
P_T	—	Total pressure *mm Hg*
P_v	—	Vapor pressures *mm Hg*
Q	—	Heat-transfer rate *W*
S	—	Humidifier cross-section m^2
T	—	Temperature °C
U	—	Overall heat-transfer coefficient $W/m^2\ °C$
V	—	Humidifier volume m^3
Z	—	Fill height *m*
a	—	Surface area per unit volume m^{-1}
c	—	Specific heat *kJ/kg °C*
d_e	—	Equivalent diameter *mm*
d_i	—	Tube inside diameter *mm*
f	—	Enthalpy correction factor *kJ/kg*
h	—	Convective heat-transfer coefficient $kJ/s\ m^2\ °C$
h_c	—	Shell-side condensate-film local heat-transfer coefficient $kJ/s\ m^2\ °C$
h_{fg}	—	Latent heat of water evaporation at ambient conditions *kJ/kg*
h_g	—	Shell-side gas-film local heat-transfer coefficient $kJ/s\ m^2\ °C$
i	—	Interest rate %
m	—	Flow rate *Kg/s*
k	—	Thermal conductivity *W/m °C*
k_w	—	Wall thermal conductivity *W/m °C*
n	—	Number of years
r_i	—	Inner radius *m*
r_o	—	Outer radius *m*
u_{cw}	—	Cooling water velocity *m/s*

Greek

α	—	Thermal diffusivity m^2/s
η_H	—	Humidifier efficiency %
η_{THD}	—	Humidifier thermal efficiency %
μ	—	Dynamic viscosity *kg/m s*
ρ	—	Density kg/m^3
ω	—	Absolute humidity kg_{water}/kg_{air}

Subscripts

DH	—	Dehumidifier
HD	—	Humidifier
a	—	Air
as	—	Saturated air
avg	—	Average value
cw	—	Cooling water
d	—	Product water
lm	—	Log mean
m	—	Mean value
mu	—	Makeup
v	—	Vapor
w	—	Water

References

[1] M. Schorr, Desalination trends and technologies, In Tech, Rijeka, 2011.
[2] S.A. El-Agouz, A new process of desalination by air passing through seawater based on humidification de-humidification process, Energy, 35 (2010) 5108–5114.
[3] M. Mehrgoo, M. Amidpour, Constructal design and optimization of a direct contact humidification–dehumidification desalination unit, Desalination, 293 (2012) 69–77.
[4] A.E. Kabeel, E.M.S. El-Said, A hybrid solar desalination system of air humidification–dehumidification and water flashing evaporation: Part I. A numerical investigation, Desalination, 320 (2013) 56–72.
[5] A.E. Kabeel, E.M.S. El-Said, A hybrid solar desalination system of air humidification dehumidification and water flashing evaporation: A comparison among different configurations, Desalination, 330 (2013) 79–89.
[6] R. González-Bravo, J.M. Ponce-Ortega, M.M. El-Halwagi, Optimal design of water desalination systems involving waste heat recovery, Ind. Eng. Chem. Res., 56(7) (2017)1834–1847.
[7] S. Atilhan, A. Bin-Mahfouz, B. Batchelor, P. Linke, A. Abdel-Wahab, F. Nápoles-Rivera, A. Jiménez-Gutiérrez, M.M. El-Halwagi, A systems-integration approach to the optimization of macroscopic water desalination and distribution networks: a general framework applied to Qatar's water resources, Clean Technol. Environ. Policy, 14(2) (2012) 161–171.
[8] R.E. Treybal, Mass transfer operations, McGraw-Hill, New York, 1980.
[9] W.L. McCabe, J.C. Smith, P. Harriott, Unit Operations of Chemical Engineering, McGraw-Hill, New York, 1993.
[10] M. Kutz, Heat Transfer Calculations, McGraw-Hill ,2004.
[11] M.H. Sharqawy, M.A. Antar, S.M. Zubair, A.M. Elbashir, Optimum thermal design of humidification dehumidification desalination systems. Desalination, 349 (2014) 10–21.

[12] H. Jaber, B.L. Webb, Design of cooling towers by the effectiveness-NTU method, ASME J. Heat Transfer, 111 (1989) 837–843.
[13] D.G. Kröger, Air-cooled heat exchangers and cooling towers. thermal-flow performance evaluation and design, PennWell Corporation, Tulsa, OK, 2004.
[14] N.K.H. Nawayseh, M.M. Farid, A. Omar, A. Sabirin, Solar desalination based on humidification process-II. Computer simulation, Energy Conver. Manage., 40 (1999) 1441–1461.
[15] M.M. Farid, S. Parekh, J.R. Selman, S. Al-Hallaj, Solar desalination with humidification-dehumidification cycle: mathematical modeling of the unit, Desalination, 151 (2003) 153–164.
[16] J. Hermosillo, A.A. Camilo, C.A. Estrada, Water desalination by air humidification: Mathematical model and experimental study, Solar Energy, 86 (2012) 1070–1076.
[17] A. Eslamimanesh, M.S. Hatamipour, Mathematical modeling of a direct contact humidification–dehumidification desalination process, Desalination, 237 (2009) 296–304.
[18] T. Mizushina, N. Hashimoto, M. Nakajima, Design of cooler condensers for gas-vapour mixtures, Chem. Eng. Sci., 9 (1959) 195–204.
[19] ASHRAE Handbook — Fundamentals Volume, ASHRAE 1791 Tullie Circle, Atlanta, GA, USA. 2001.
[20] P.F. Incropera, D.P. Dewitt, T.L. Bergman, A.S. Lavine, Fundamentals of heat and mass transfer, John Wiley and Sons, Danvers, MA, 2007.
[21] L.S. Lasdon, R.L. Fox, M.W. Ratner, Nonlinear optimization using the generalized reduced gradient method. Revue française d'automatique, informatique, recherche opérationnelle, Recherche opérationnelle, 8(V3) (1974) 73–103.
[22] K.R. Baker, Optimization Modeling with Spreadsheets, John Wiley and Sons, Hoboken, NJ, 2012.
[23] M. Graueer, G. Gruhn, L. Pollmer, Optimization of a complex plant by a GRG algorithm, Comp. Chem. Eng., 3(1–4) (1979) 597–602.
[24] R. Adamson, M. Hobbs, A. Silcock, G. Montague, Real time optimisation of industrial gas supply networks, IFAC-PapersOnLine, 48(8) (2015) 355–360.
[25] S. Farsad, A. Behzadmehr, Analysis of a solar desalination unit with humidification–dehumidification cycle using DoE method, Desalination, 278(1–3) (2011) 70–76.
[26] A.M.I. Mohamed, N.A. El-Minshawy, Theoretical investigation of solar humidification–dehumidification desalination system using parabolic trough concentrators, Energy Convers. Manage., 52(10) (2011) 3112–3119.
[27] A.E. Kabeel, M.H. Hamed, Z.M. Omara, S.W. Sharshir, Water desalination using a humidification-dehumidification technique—a detailed review, Nat. Resour., 4(3) (2013) 286–305.
[28] F. Abdel-Hady, M.M. El-Halwagi, M. Alghamdi, A.K. Mazher A. Alzahrani, Experimental study of humidification and dehumidification desalination process, Int. J. Eng. Technol., 10(2) (2018) 511–528.
[29] A.Y. Cenegel, M.A. Boles, Thermodynamics: An Engineering Approach, McGraw-Hill, New York, NY, 2015.
[30] C.J. khisty, J. Mohammadi, A.A. Amekudzi, Systems engineering with economics, Probability, and Statistics, J. Ross Publishing, Lauderdale, FL, 2012.
[31] Saudi electricity company official web site, https://www.se.com.sa/en-us/Customers/Pages/TariffRates.aspx
[32] G. Towler, R.K. Sinnott, Chemical engineering design: Principles, Practice and Economics of Plant and Process Design, Elsevier Butterworth-Heinemann: Burlington, MA, 2008.
[33] G.P. Rangaiah, Multi-objective optimization: Techniques and Applications in Chemical Engineering, World Scientific Publishing Co. Pte. Ltd., Hackensack, NJ, 2009.
[34] T. Rajaseenivasan, K. Srithar, An investigation into a laboratory scale bubble column humidification dehumidification desalination system powered by biomass energy, Energy Convers. Manage., 139 (2017) 232–244.
[35] E. Deniz, S. Çınar, Energy, exergy, economic and environmental (4E) analysis of a solar desalination system with humidification-dehumidification, Energy Convers. Manage., 126 (2016) 12–19.
[36] H.A. Ahmed, I.M. Ismail, W.F. Saleh, M. Ahmed, Experimental investigation of humidification-dehumidification desalination system with corrugated packing in the humidifier, Desalination, 410 (2017) 19–29.
[37] S.A. El-Agouz, A new process of desalination by air passing through seawater based on humidification–dehumidification process, Energy, 35(12) (2010) 5108–5114.
[38] Z. Rahimi-Ahar, M.S. Hatamipour, Y. Ghalavand, Solar assisted modified variable pressure humidification-dehumidification desalination system, Energy Convers. Manage., 162 (2018) 321–330.
[39] M.H. Hamed, A.E. Kabeel, Z.M. Omara, S.W. Sharshir, Mathematical and experimental investigation of a solar humidification–dehumidification desalination unit, Desalination, 358 (2015) 9–17.
[40] P. Behnam, M.B. Shafii, Examination of a solar desalination system equipped with an air bubble column humidifier, evacuated tube collectors and thermosyphon heat pipes, Desalination, 397 (2016) 30–37.
[41] M.B. Shafii, H. Jafargholi, M. Faegh, Experimental investigation of heat recovery in a humidification-dehumidification desalination system via a heat pump, Desalination, 437 (2018) 81–88.
[42] R.K. Sinnott, Coulson and Richardson's Chemical Engineering, Chemical Engineering Design, Elsevier Butterworth-Heinemann, Oxford, UK, 2005.
[43] K.S. Wang, Handbook of air conditioning and refrigeration, McGraw-Hill, New York, NY, 2001.
[44] F. Kreith, The CRC handbook of thermal engineering, CRC Press, Boca Raton, FL, 2000.
[45] M. Mehrgoo, M. Amidpour, Derivation of optimal geometry of a multi-effect humidification–dehumidification desalination unit: A constructal design, Desalination, 281 (2011) 234–242.
[46] D.Q. Kern, Process Heat Transfer, McGraw Hill, Tokyo, 1965.
[47] J.M. Coulson, J.F. Richardson, Coulson and Richardson's Chemical Engineering, Fluid Flow, Heat Transfer and Mass Transfer, Butterworth-Heinemann, Woburn, MA, 1999.
[48] A.E. Kabeel, E.M.S. El-Said, Applicability of flashing desalination technique for small scale needs using a novel integrated system coupled with nanofluid-based solar collector, Desalination, 333 (2014) 10–22.

Appendix A

Thermodynamic relations.

Vapor pressure of pure liquids can be calculated with the Antoine equation with a temperature range of 11–168°C [42]:

$$Ln\,Pv = 18.3036 - \frac{3816.44}{227.02 + T(^{\circ}C)} \tag{8}$$

Absolute humidity is defined as kg of vapor contained in 1 kg of dry air. Humidity depends on the partial pressure of water vapor in the air and on the total pressure [29].

$$\omega = 0.62\frac{P_v}{P_T - P_v} \tag{9}$$

Enthalpy of humid air is described as the total heat of a 1 kg mixture of water vapor and dry air and presented in J/kg [29].

$$H_a = \left[C_a T_a + 597.2\omega\right] \times 4186.8 \tag{10}$$

Specific heat of humid air is defined as the amount of heat required to increase or decrease the temperature of a 1 kg dry-air and water-vapor mixture by 1°C [43].

$$C_a = \left[0.24 + 0.46\omega_S\right] \tag{11}$$

Appendix B

The thermophysical properties of dry air at a range of 220–380 K at standard atmospheric pressure (101,325 N/m²) [13]

Density in kg/m³

$$\rho_a = \frac{p_a}{287.08T} \tag{12}$$

Dynamic viscosity in kg/sm

$$\mu_a = 2.287973\times10^{-6} + 6.259793\times10^{-8}T - 3.131956\times10^{-11}T^2 + 8.15038\times10^{-15}T^3 \tag{13}$$

Thermal conductivity in W/m K

$$k_a = 4.937787\times10^{-4} + 1.018087\times10^{-4}T - 4.627937\times10^{-8}T^2 + \times10^{-11}T^3 \tag{14}$$

Specific heat in J/kg K

$$C_a = 1.045356\times10^{-6} - 3.161783\times10^{-1}T + 7.083814\times10^{-4}T^2 - 2.705209\times10^{-7}T^3 \tag{15}$$

Appendix C

The thermophysical properties of saturated water vapor from 273.15 to 380 K [13]

Density in kg/m³

$$\rho_v = -4.062329.56 + 0.10277044\times T - 9.76300388\times10^{-4}T + 7.083814\times10^{-4}T^2 + 4.475240795\times10^{-6}T^3 - 1.004536894\times10^{-8}T^4 + 8.9154895\times10^{-12}T^5 \tag{16}$$

Dynamic viscosity in kg/sm

$$\mu_v = 2.562435\times10^{-6} + 1.816683\times10^{-8}T + 2.579066\times10^{-11}T + 7.083814\times10^{-4}T^2 - 1.067299\times10^{-14}T^3 \tag{17}$$

Thermal conductivity in W/m K

$$k_v = 1.3046\times10^{-2} - 3.756191\times10^{-5}T + 2.217964\times10^{-7}T^2 - 1.111562\times10^{-10}T^3 \tag{18}$$

Specific heat in J/kg K

$$C_v = 1.3605\times10^{3} + 2.31334\times T - 2.46784\times10^{-10}T^5 + 5.91332\times10^{-13}T^6 \tag{19}$$

Appendix D

Mass- and heat-transfer coefficients

The experimental mass-transfer coefficient is correlated [28] and given by the following equation.

$$K_y aV = 0.5195\left(\frac{m_{W1}}{m_a}\right)^{-0.708} \tag{20}$$

Dehumidifier overall heat-transfer coefficient [20,42,44]:

$$\frac{1}{U_{DH}} = \frac{1}{h_{CW}} + \frac{r_i}{K_W}\ln\left(\frac{r_o}{r_i}\right) + \frac{r_i}{r_o h_a} \tag{21}$$

Dehumidifier tube-side heat-transfer coefficient [42]:

$$h_{CW} = \frac{4200\left(1.35 + 0.02T_{CW}\right)u_{CW}^{0.8}}{d_i^{0.2}} \tag{22}$$

Dehumidifier shell-side heat-transfer coefficient [42,45]:

$$\frac{1}{h_a} = \frac{1}{h_c} + \frac{Y}{h_g} \tag{23}$$

where Y is expressed as follows:

$$Y = C_a\frac{\Delta T_a}{\Delta H_a} \tag{24}$$

Dehumidifier air-film heat-transfer coefficient [46,47]:

$$\frac{h_g d_e}{k_a} = 0.36\,\mathrm{Re}^{0.55}\,\mathrm{Pr}^{\frac{1}{3}}\left(\frac{\mu_a}{\mu_v}\right)^{0.14} \tag{25}$$

For the designed square-pitch arrangement, the following parameters were calculated:

$$d_e = \frac{1.27}{d_o}\left(p_t^2 - 0.785 d_0^2\right) \tag{26}$$

Dehumidifier condensate-film heat-transfer coefficient [46,47]:

$$h_c\left(\frac{\mu_v^2}{k_v^3 \rho_v^2 g}\right)^{\frac{-1}{3}} = 1.47\left(\frac{4M}{\mu_v}\right)^{\frac{-1}{3}} \tag{27}$$

Mass flow rate per unit length of perimeter M is calculated with the following relation:

$$M = \frac{m_d}{N_t \pi d_o} \tag{28}$$

Appendix E

Performance parameters

Humidifier efficiency:

$$\eta_H = 100 \times \left(\frac{\omega_{a2} - \omega_{a1}}{\omega_s - \omega_{a1}}\right) \tag{29}$$

GOR:

$$GOR = \frac{m_d h_{fg}}{Q_{in}} \tag{30}$$

Humidifier thermal efficiency [29]:

$$\eta_{T_{HD}} = 1 - \frac{Q_{out\,HD}}{Q_{in}} \tag{31}$$

$$Q_{out\,HD} = m_a\left(H_{a2} - H_{a1}\right) \tag{32}$$

Appendix F

Dehumidifier energy balance:

$$m_a\left(H_{a2} - H_{a1}\right) = m_{cw} C_w \left(T_{cw2} - T_{cw1}\right) + m_d C_w T_{w1} - Q_{HD\,loss} \tag{33}$$

Humidifier energy balance:

$$m_a\left(H_{a2} - H_{a1}\right) = m_{w2} C_w T_{w2} - m_{w1} C_w T_{w1} - Q_{HD\,loss} \tag{34}$$

Appendix G

Cost analysis

Total operating cost [48]:

$$C_{TOP} = C_A + C_{OP} + C_M \tag{35}$$

Annual capital cost [30]:

$$Annual\,capital\cos t\left(C_A\right) = P\frac{\left[i(1+i)^n\right]}{\left[(1+i)^n - 1\right]} \tag{36}$$

Unit production cost:

$$Production\cos t = \frac{Total\,production\cos t\left(C_{TOP}\right)}{Annaul\,production}\frac{US\$}{m^3} \tag{37}$$